Chemical Engineering Journal 163 (2010) 389–394

Contents lists available at ScienceDirect

Chemical Engineering Journal

journal homepage: www.elsevier.com/locate/cej

# Characterization of coke deposited on spent catalysts for long-chain-paraffin dehydrogenation

Songbo He [a], Chenglin Sun [a,*], Xu Yang [a], Bin Wang [b], Xihai Dai [b], Ziwu Bai [b]

[a] Dalian National Laboratory for Clean Energy, Dalian Institute of Chemical Physics, Chinese Academy of Sciences, Dalian, Liaoning 116023, PR China
[b] PetroChina Fushun Petrochemical Company, Fushun, Liaoning 113001, PR China

ARTICLE INFO

*Article history:*
Received 28 January 2010
Received in revised form 20 June 2010
Accepted 9 July 2010

*Keywords:*
Dehydrogenation
Coke
Deactivation
Long chain paraffin
Pt-Sn catalysts

ABSTRACT

The chemistry, morphology, and structure character of coke deposited on spent catalysts for long-chain-paraffin ($n$-$C_{16-19}$) dehydrogenation and the effect of coke on the surface structure of the catalysts were studied by several characterization techniques: thermogravimetry/differential thermal analysis (TG-DTA), elemental analysis, UV Raman spectroscopy, temperature-programmed oxidation (TPO), scanning electron microscopy (SEM), X-ray diffraction (XRD), Brunaucr–Emmett–Teller (BET), mercury intrusion porosimetry (MIP) and CO-chemisorption. During the dehydrogenation of $n$-$C_{16-19}$, coke gradually accumulates on the surfaces of the catalysts while the coking rate and the H/C mole ratio of the coke decrease. After the times on stream (TOS) of 960 h, the coke deposition on the catalysts is up to 6.56 wt.%, and the H/C mole ratio of the coke is only 0.86. The coke is graphited or amorphous nature and contains conjugated olefinic species and polycyclic aromatic hydrocarbons (PAHs). The coke causes a significant deactivation of the active sites. As compared with the fresh catalysts, the surface area, the total pore volume and the Pt dispersion of the spent catalysts are decreased 19.4%, 33.3% and 61.2%.



## 1. Introduction

Dehydrogenation of long chain paraffins ($n$-$C_{10-13}$ and $n$-$C_{16-19}$) to olefins is an important catalytic process of producing linear alkylbenzene sulfonate (LABS) for biodegradable detergents [1,2] and heavy alkylbenzene sulfonate (HABS) for the enhanced oil recovery [3,4]. The catalysts employed are Pt-Sn bimetallic supported $Al_2O_3$ catalysts. Generally, the lifetime of the commercial long-chain-paraffin dehydrogenation catalysts (e.g., DEH-7 type of catalysts, UOP LLC, U.S. and DF type of catalysts, PFPC, China) is only 40–60 days [5,6]. The spent catalysts deactivated by coking should be unloaded, followed by being regenerated or discharged after the recovery of Pt. It is not convenient and economic for the industrial production. Therefore, it is very important to understand the characteristics and the formation mechanism of the coke, as well as the process for regeneration of the long-chain-paraffin dehydrogenation catalysts.

Deactivation of Pt-Sn bimetallic catalysts by coke deposition has been extensively investigated by a number of authors and most of them were concentrated on: kinetics of coke deposition [7–9]; structure of coke [10,11]; chemical nature of coke [12–14]; location of the coke deposition [10,11,15–17]; effect on different catalytic sites and catalyst performance [7,18,19] and burning-off the coke for the catalyst recovery [6,20]. It is well established that coke formation depends on the operating conditions [11,13,21–23], such as the nature of the reaction, the type of catalysts, the reactor feedstock composition, temperature, pressure and times on stream (TOS). The coke formation involves the metallic function (dehydrogenating capacity) and acidic function (condensation–polymerization capacity) of the catalysts with the steps of dehydrogenation, condensation, alkylation and cyclization [8,24]. The coke species may include elemental carbon, graphitized carbon and high molecular weight polymeric carbon [13,24], and the structure of coke can be grouped into amorphous, filamentous and graphitic platelets [25]. The coke deposition may locate on the metal sites and support surface [15,16]. It was also found that coke initially deposited on metallic sites, and the quantity of carbon on metallic sites did not change much with reaction time [23,26]. The coke deposition on the metallic sites is rich in hydrogen. While the coke deposited on the support is more dehydrogenated [12] and graphite like [27].

The chemistry and structural characterization of the coke deposits on the catalysts after industrial dehydrogenation of $n$-$C_{10-13}$ had been discussed by Afonso et al. [13] and Sahoo et al. [28] earlier. Now the new type of catalyst for the dehydrogenation of $n$-$C_{16-19}$ is under developing [4], and there are no reports on the characterization of the coke during the dehydrogenation of $n$-$C_{16-19}$. An in-depth understanding of the coke characterization and the coking process is helpful to improve the performance of the catalysts for the dehydrogena-

* Corresponding author. Tel.: +86 411 84379133; fax: +86 411 84699965.
*E-mail address:* clsun@dicp.ac.cn (C. Sun).

1385-8947/$ – see front matter © 2010 Elsevier B.V. All rights reserved.
doi:10.1016/j.cej.2010.07.024

**Table 1**
Process conditions, carbon content, elemental analysis and UV Raman spectra analysis data of spent catalysts.

| Sample code | Times on stream (h) | Average conversion (%, w/w) | Carbon content[a] (%, w/w) | H/C ratio[b] (mol/mol) | $I(D)/I(G)$[c] |
|---|---|---|---|---|---|
| CDH-1 | 10 (455–455 °C) | 17.97 | 2.46 | 1.64 | 0.67 |
| CDH-2 | 36 (455–455 °C) | 17.61 | 4.97 | 1.23 | 0.65 |
| CDH-3 | 240 (455–461 °C) | 13.43 | 5.38 | 1.19 | 0.66 |
| CDH-4 | 960 (455–484 °C) | 11.52 | 6.56 | 0.86 | 0.47 |

[a] TG-DTA.
[b] Elemental analysis.
[c] UV Raman spectra analysis.

tion of $n$-$C_{16–19}$ and to investigate the catalyst regeneration technology.

In this contribution, the characterization of the coke deposited on the Pt-Sn-K/γ-$Al_2O_3$ catalysts during the dehydrogenation of $n$-$C_{16–19}$ was investigated. What we concerned about was (1) the effect of TOS and processing parameters on the catalyst deactivation and the coke formation; (2) the chemistry and structure of coke deposition; and (3) the effect of coke on the dehydrogenation reaction and the surface structure of the catalysts.

## 2. Experimental

### 2.1. Catalysts and dehydrogenation process

The catalysts used in this study were $Pt_{0.2}$-$Sn_{0.6}$-$K_{0.2}$/$Al_2O_3$ catalysts (hereafter designated as CDH-0) prepared by the vacuum complex impregnation method [4]. Before the impregnation, the alumina samples were outgassed for 30 min. Then the impregnation solution, which contains $H_2PtCl_6$, $SnCl_2$, KCl and HCl, was impregnated onto the alumina supports, and the mixture was kept gently stirred for 30 min, followed by vacuuming at 60–70 °C. Then the catalysts were dried at 120 °C overnight and finally calcined at 520 °C in air for 8 h.

The catalytic dehydrogenation of $n$-$C_{16–19}$ (industry grade, Cangzhou Jincang Chemical Corporation Limited Hebei, China) was carried out on a fixed bed micro-catalytic reactor [4]. The catalysts (2.5 mL) were first reduced at 470 °C for 4 h, followed by being cooled to 380 °C in $H_2$ (purity 99.995%) atmosphere. The $n$-paraffins were then pumped into the reactor, and the temperature was programmed up to the reaction temperature within 60 min. The LHSV of the $n$-paraffins was 20 $h^{-1}$ and GHSV of hydrogen was 12,000 $h^{-1}$. The reaction pressure was controlled at 0.14 MPa, the reaction temperature was 455–484 °C.

### 2.2. Spent catalyst sample collection

When the period of the dehydrogenation reaction was completed, the $n$-$C_{16–19}$ flow was stopped and the catalyst bed temperature was cooled down to 50 °C accompanied with the normal flow of hydrogen. Then the gas flow was switched to nitrogen (purity 99.99%), and the catalyst bed temperature gradually fell to ambient conditions. The spent catalysts were unloaded, and named as CDH-1, CDH-2, CDH-3 and CDH-4, according to TOS (Table 1). The specimens of the used catalysts (2.5 mL) were then purged in Ar (99.99%, 500 mL $min^{-1}$) at 485 °C for 1 h to remove any adsorbed materials for the catalyst characterization and coke analysis.

### 2.3. Catalyst characterizations

The carbon content of the used catalysts was measured by a thermogravimetry/differential thermal analysis (TG-DTA) instrument (SETSYS 16/18, France) from room temperature to 800 °C at a heating rate of 10 °C $min^{-1}$ in an air flow of 50 mL $min^{-1}$. α-$Al_2O_3$ was used as a reference.

The amount of C and H element of the coke was determined using a vario EL III universal CHNOS elemental analyzer (Elementar Analysensysteme GmbH, Hanau, Germany).

The ultraviolet (UV) Raman spectra were collected at room temperature on a Jobin-Yvon T64000 triple-stage spectrograph (Paris, France) with spectral resolution of 2 $cm^{-1}$. The laser line at 325 nm of a He–Cd laser was used as an excitation source with an output of 25 mW. The power of laser at the sample was about 3.0 mW.

Temperature-programmed oxidation (TPO) analysis of the deactivated catalysts was carried out using a Micromeritics AutoChem II 2920 apparatus (American). Prior to the measurement, the samples were pretreated in He (99.99%, 20 mL $min^{-1}$) at 485 °C for 1 h. After cooling to room temperature in He, the gas flow was switched to 2% $O_2$ in He and the samples were heated from room temperature to 800 °C with a temperature ramp of 10 °C $min^{-1}$. The $O_2$ consumption and $CO_2$ output were determined by an on-line quadrupole mass analyzer (Omnistar, Balzers, Vaduz, Liechtenstein).

Scanning electron microscopy (SEM) experiments were performed on a scanning electron microscope (Quanta 200F, FEI Company) with an accelerating voltage of 20 kV.

The crystallinity of the samples was analyzed by powder X-ray diffraction (XRD, Rigaku D/max-γB powder diffractometer, Japan) with Cu Kα radiation at 40 kV and 40 mA in the scan $2\theta$ range of 10–80°.

The Brunaucr–Emmett–Teller (BET) surface areas were calculated from the adsorption isotherms of nitrogen at 77 K on a volumetric adsorption system (Micromeritics ASAP 2010, American). All samples were degassed at 200 °C before BET measurements.

Mercury intrusion porosimetry (MIP) analysis was generated using a mercury porosimeter (Micromeritics Autopore 9520, American). Samples were outgassed in vacuum (0.01 Torr) for 1 h at 95 °C. An arbitrary mercury contact angle of 130° and a surface tension of 485 dyn $cm^{-1}$ were used to calculate pore size distribution (PSD) data from the mercury intrusion–extrusion curves.

Pulse chemisorption of CO (CO-chemisorption) experiment was performed to analyze the Pt dispersion in the catalysts (Micromeritics AutoChem II 2920, American). The samples were reduced under $H_2$ (99.99%, 20 mL $min^{-1}$) at 500 °C for 1 h, then purged in He (99.99%, 20 mL $min^{-1}$) at 520 °C for 1 h and cooled down to 50 °C in flowing He (20 mL $min^{-1}$). The 0.1 $cm^3$ pulses of a mixture of CO in He (5%) were sent to the reactor, and the time between pulses was 4 min.

## 3. Results and discussion

### 3.1. Catalyst deactivation and the coke formation

The coke deposited on the deactivated long-chain-paraffin ($n$-$C_{16–19}$) dehydrogenation catalysts was quantitatively analyzed by TG analysis. The dehydrogenation process (the reaction temperature range, the average conversion and TOS) and the coke deposition amount are presented in Table 1. The analysis of the coke deposited on the long-chain-paraffin ($n$-$C_{16–19}$) dehydrogenation catalysts presents the dynamic process of the coke deposition.

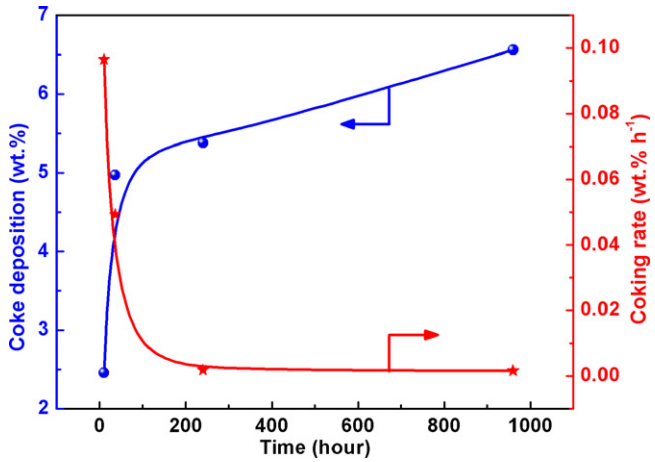


**Fig. 1.** Dependence of the carbon deposition and coking rate on TOS during the dehydrogenation of $n$-$C_{16-19}$ paraffins.

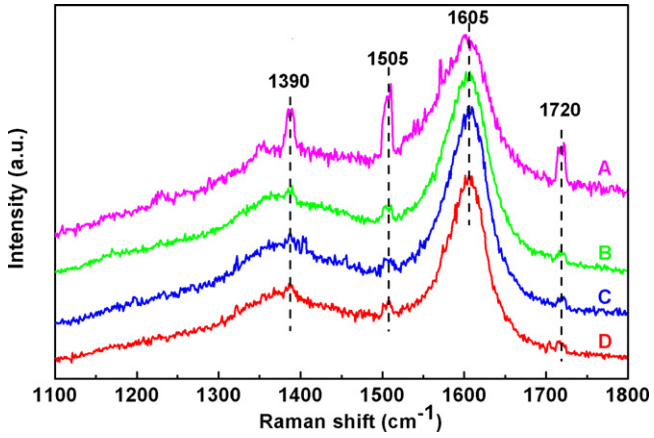


**Fig. 2.** UV Raman spectra of the deactivated catalysts (A) CDH-1, (B) CDH-2, (C) CDH-3 and (D) CDH-4.

During the preliminary reaction time of 10 h, the amount of the coke deposited on the catalysts (CDH-1) is 2.46 wt.%. After the successive reaction time of 36 h, the coke amount of the catalysts (CDH-2) reaches a very high level (4.97 wt.%). And 240 h later, the amount of coke on the catalysts (CDH-3) is 5.38 wt.%. The catalysts deactivated very quickly due to the coke deposition, and the average conversion of the catalysts was declined from 17.61 wt.% of the initial 36 h to 13.43 wt.% of the 240 h, although the increased reaction temperature was restored to remain the activity of the catalysts. After the TOS of 960 h, the coke deposition on the catalysts (CDH-4) is accumulated up to 6.56 wt.%, and the average conversion of the catalysts is dropped to 11.52 wt.%.

Coking is one of the side reactions of the long-chain-paraffin dehydrogenation reaction. The amount of the coke deposition is significantly affected by the dehydrogenation operation conditions, such as the reaction temperature, the overall average conversion and the TOS. Generally, the higher the reaction temperature and the reaction activity are, the more easily the coke is formed. Moreover, the coke formation is an accumulative process. The relationship of coke deposition and TOS during the dehydrogenation of $n$-$C_{16-19}$ is illustrated in Fig. 1. It can be observed that with the prolongation of the dehydrogenation reaction, the amount of coke deposition on the catalysts was increased, while the increment of coke was decreased. Similar results can be observed in other reports [29]. During the initial stage of the reaction, the dehydrogenation activity of the catalysts is very high, which tends to cause the deep dehydrogenation reaction and coking easily. The plot of coking rate versus TOS, which was obtained by differentiating the dependence curve of coke deposition and TOS, was also depicted in Fig. 1. It is clearly shown that the coking rate is very fast at the initial reaction stage. With the proceeding of the reaction, the active sites and acidic centers of the catalysts are gradually covered by coke, and the active centers for the coke reaction are decreased so that the velocity of coke formation drops markedly.

### 3.2. Coke nature, structure and location

#### 3.2.1. Elemental analysis

The elemental analysis data of the deactivated long-chain-paraffin ($n$-$C_{16-19}$) dehydrogenation catalysts are listed in Table 1. It can be observed that during the dehydrogenation of $n$-$C_{16-19}$, with the reaction proceeding, the coke loading was increased while the H/C mole ratio of coke was decreased, which indicated that with the increasing of TOS, the degree of coking was increased and the coke was more and more graphited in nature. Similar results were also reported by Barbier [30]. After the TOS of 36 h in the dehydrogenation of $n$-$C_{16-19}$, the H/C mole ratio of the coke on the CDH-2 catalysts is 1.23. While 40 days later, the H/C mole ratio of the coke on the CDH-4 catalysts is only 0.86.

#### 3.2.2. UV Raman spectra analysis

The TG and elemental analysis can only give the information of the total amount and H/C mole ratio of the coke on the catalysts, and help to present the general view of the coke deposition. To distinguish the chemical nature of the coke deposited on the long-chain-paraffin ($n$-$C_{16-19}$) dehydrogenation catalysts, UV Raman spectroscopy was first employed, and the UV Raman spectra of the deactivated catalysts are shown in Fig. 2. It can be seen from Fig. 2 that several Raman bands appear at 1390, 1505, 1605 and 1720 cm$^{-1}$. The band at 1390 and 1605 cm$^{-1}$ are assigned to so-called G and D peaks, which are due to $sp^2$ carbon species [31]. The G peak is due to the bond stretching of all pairs of $sp^2$ atoms in both rings and chains, and the D peak is due to the breathing modes of $sp^2$ atoms in rings. These two peaks are common for various forms of disordered, noncrystalline, and amorphous carbons in the Raman spectra [32]. It can be observed that the band at 1582 cm$^{-1}$ of the crystalline graphite shifts to higher frequencies 1607 cm$^{-1}$ in the deactivated long-chain-paraffin dehydrogenation catalysts, which is possibly related to conjugated olefinic species or polycyclic aromatic hydrocarbons (PAHs) [32,33]. And the different PAHs also exhibit UV Raman peaks in the spectral region where the D peak is located [32,34]. Thus, it can be deduced that the coke on the deactivated long-chain-paraffin ($n$-$C_{16-19}$) dehydrogenation catalysts is the deep-dehydrogenated carbonaceous compounds, which includes conjugated olefinic species and PAHs. The intensity ratio of the D peak to the G peak ($I$(D)/$I$(G)) was also calculated and listed in Table 1. It can be observed that the ratio of $I$(D)/$I$(G) for CDH-4 is 0.47 and lower than the ratios of $I$(D)/$I$(G) for CDH-1, CDH-2, and CDH-3. The results indicate that the degree of graphitization or amorphous nature of the coke deposited on CDH-4 is more than those on CDH-1, CDH-2, and CDH-3.

#### 3.2.3. TPO analysis

The deactivated long-chain-paraffin ($n$-$C_{16-19}$) dehydrogenation catalysts were also subjected to TPO analysis and the TPO profiles are given in Fig. 3. TPO peaks for the deactivated catalysts (CDH-1, CDH-2, CDH-3, CDH-4) after the dehydrogenation of $n$-$C_{16-19}$ show one broad peak for coke oxidation. With the TOS of the dehydrogenation of $n$-$C_{16-19}$ prolonging, the maximum peak temperature ($T_M$) of the TPO profile shifted to higher temperature, which is indicated that the degree of the graphitization is getting higher [35]. And this is in accordance with the results of H/C mole ratio of the elemental analysis.

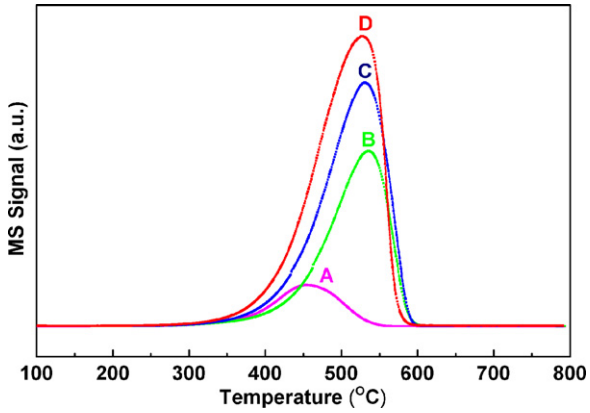


**Fig. 3.** TPO profiles of the deactivated catalysts (A) CDH-1, (B) CDH-2, (C) CDH-3 and (D) CDH-4.

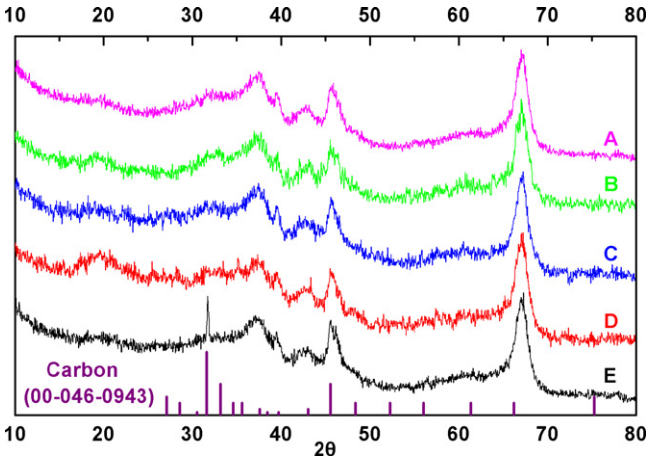


**Fig. 5.** XRD patterns of the catalysts (A) CDH-0, (B) CDH-1, (C) CDH-2, (D) CDH-3 and (E) CDH-4.

### 3.2.4. SEM imaging and XRD spectra

The morphology of the coke on the catalysts was further studied by SEM. All the deactivated catalysts are black in color, and the natural visual impression is that the catalysts were totally covered by coke. Thus it can be supposed that the images observed in the SEM are relative to the coke deposition on the catalysts [11]. Fig. 4 presents the SEM images of the CDH-4 catalysts which were deactivated during the dehydrogenation of $n$-$C_{16-19}$. SEM images of CDH-4 catalysts (Fig. 4C and D) reveal some disk-like, stacked, spherical and irregular features. The new peak at $2\theta = 31.83^\circ$ with $d$ values of 0.2830 nm in the XRD patterns of CDH-4 catalysts (Fig. 5E) indicates that a small amount of crystalline carbon has been formed on the deactivated catalysts. Due to the massive amorphous coke, it was difficult to observe the layered graphitized coke in the SEM. Based on the knowledge that the burning temperature of the amorphous coke is lower than that of the graphitized coke, Zhang et al. [27] and Zhang [36] successfully observed the graphitic layer of coke after the partial oxidation of the coke on the catalysts. And the deposited coke was aggregated preferentially around the edges of the discs with the TOS prolonging, and finally formed the graphite-like 3D structure [11,37]. Thus, the coke on the long-chain-paraffin ($n$-$C_{16-19}$) deactivated catalysts (CDH-4) is amorphous and graphitized structure.

The XRD patterns of the deactivated long-chain-paraffin ($n$-$C_{16-19}$) dehydrogenation catalysts after different TOS are shown in Fig. 5. As for CDH-1, CDH-2 and CDH-3 catalysts, with the TOS of 10, 36 and 240 h, respectively, the XRD patterns only show the diffraction peaks corresponding to the alumina supports. While after the TOS of 40 days, the XRD patterns of the CDH-4 catalysts exhibit the diffraction peak of crystalline carbon phase. It can be speculated that during the dehydrogenation of $n$-$C_{16-19}$, some of the coke species on the catalysts were gradually deep dehydrogenated and

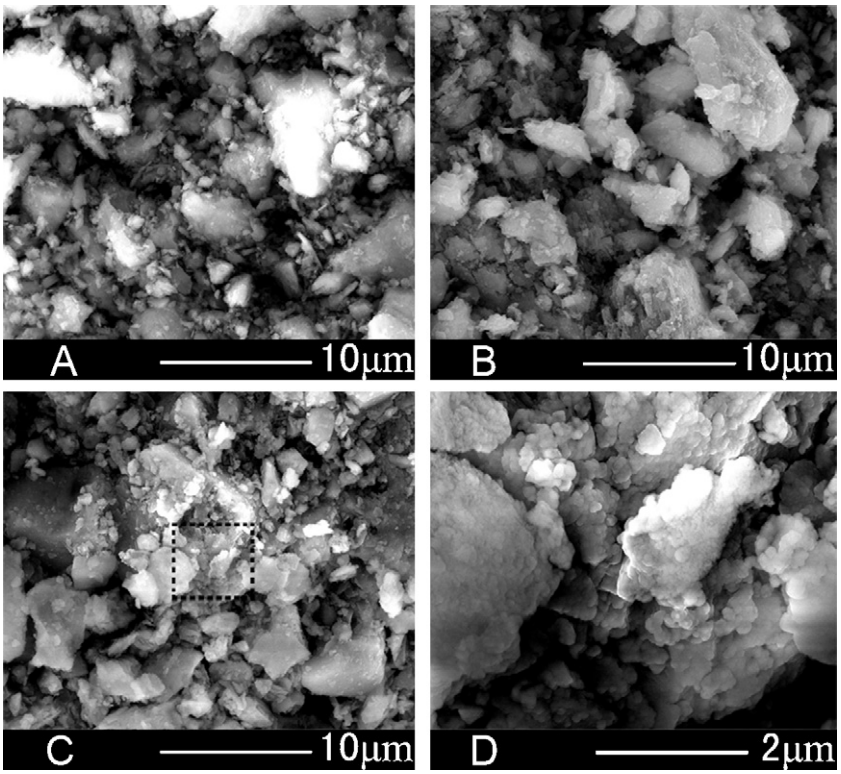


**Fig. 4.** Scan electron microscope morphologies of (A) $Al_2O_3$, (B) CDH-0, (C) CDH-4 and (D) CDH-4.

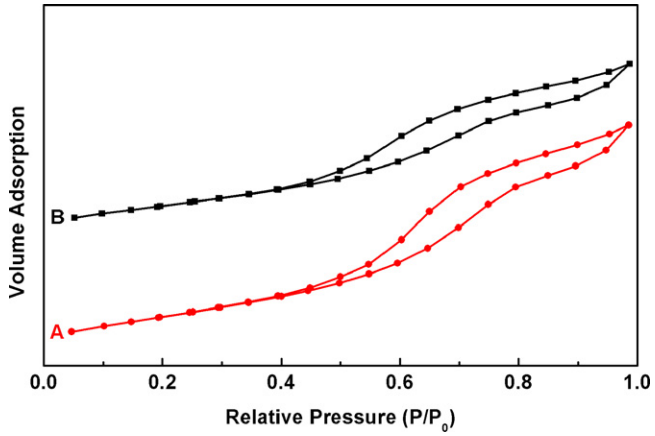


**Fig. 6.** Nitrogen adsorption/desorption isotherms of (A) CDH-0 and (B) CDH-4.

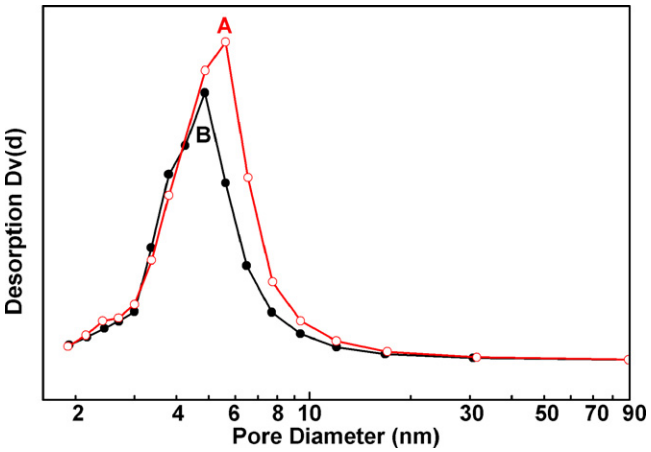


**Fig. 7.** BJH PSD of (A) CDH-0 and (B) CDH-4.

restructured, and finally formed the graphitized or pseudo-graphite structure, which is identical with the results of UV Raman analysis.

### 3.3. Effect of coke on the surface structure of the catalysts

#### 3.3.1. BET measurements and MIP analysis

BET measurements and MIP analysis were combined to investigate the textural modification after the coke deposition. As shown in Fig. 6, the nitrogen adsorption/desorption isotherms of the catalysts are type IV [38]. The hysteresis loop (Fig. 6A) of CDH-0 catalysts for the dehydrogenation of $n$-$C_{16-19}$ corresponds to type of H4, which reveals the narrow slit-shaped pores [39]. The BET isotherms of the deactivated catalysts (Fig. 6B) are almost same with that of the fresh catalysts, which indicate that no or slight changes in the pore structure of the catalysts were taken place after the coke deposition during the long-term run of the dehydrogenation.

The BET data of the fresh and deactivated catalysts are displayed in Table 2. The surface area of the deactivated catalysts will be given by: $S_{BET}\ (m^2\ g^{-1}) = W_C S_C + (1 - W_C) S_{Fresh}(1 - f)$, where $W_C$, $S_C$, $S_{Fresh}$ and $f$ stand for the weight fraction of the coke, the surface area of the coke deposition, the surface area of the fresh catalysts and the fraction of the catalyst surface covered by coke. It can be found from Table 2 that the surface area of the catalysts is decreased after the coke deposition. The change of the surface area of the catalysts after coke deposition depends not only on the coke content but also on the way in which the coke is deposited on the catalyst surface. As most of the coke deposited is flat epitaxial and layered structure, and the surface area of the coke is smaller than that of the fraction of the catalysts which covered by coke, then the surface area of the deactivated catalysts is lower than that of the fresh catalysts.

The Barrett–Joyner–Halenda (BJH) PSD of the catalysts calculated from the desorption branches of the isotherms according to the BJH method are depictured in Fig. 7. It can found that the PSD of the catalysts for the dehydrogenation of $n$-$C_{16-19}$ is shifted about 0.75 nm to lower pore diameters.

In order to access the changes of PSD of the catalysts after the coke deposition comprehensively, MIP analysis was also performed, and the MIP PSD curves of the catalysts are displayed in Fig. 8. The PSD of the fresh catalysts (Fig. 8A) exhibits an obvious bimodal distribution with one centered in the mesoporous range (4.6 nm) and the other in the macroporous range (800 nm). After the coke deposition, the total pore volume of the catalysts is decreased to some degree, and the PSD is appreciably shifted to smaller pore diameters.

It can be concluded from the BET measurements and MIP analysis that the coke decreases the surface area and the total pore volume of the catalysts, and narrows the pore size to smaller values. And the coke deposition process might be a pore-blocking action [40].

#### 3.3.2. CO pulse chemisorption

Pulse chemisorption of CO experiment was performed to analyze the Pt dispersion of the fresh and deactivated catalysts, and the Pt dispersion data are listed in Table 2. The Pt dispersion of the fresh catalysts for the dehydrogenation of $n$-$C_{16-19}$ is 72.7%. But after the long-term operation of the dehydrogenation, the Pt dispersion of the catalysts for the dehydrogenation of $n$-$C_{16-19}$ is decreased about 60%.

In fact, the dehydrogenation catalysts are not absolutely deactivated by coke. The conversion of the dehydrogenation of $n$-$C_{16-19}$ on the CDH-4 catalysts are about 10 wt.% after the TOS of 40 days. During the industrial dehydrogenation process, when the yield of the target products (linear alkylbenzene) is below the desirable value, or the energy consumption is relative high and the ratio of output and input is not sufficient anymore, the catalysts will then be considered deactivated. As mentioned above, the coke deposi-

**Table 2**
Characterization of the fresh and deactivated Pt-Sn-K/$Al_2O_3$ catalysts.

| Catalysts | $S_{BET}$ ($N_2$) ($m^2\ g^{-1}$) | Pore volume[a] ($cm^3\ g^{-1}$) | Pt dispersion[b] (%) |
|---|---|---|---|
| CDH-0 | 151.9 | 0.60 | 72.7 |
| CDH-4 | 122.4 | 0.40 | 28.2 |

[a] MIP.
[b] CO pulse chemisorption.

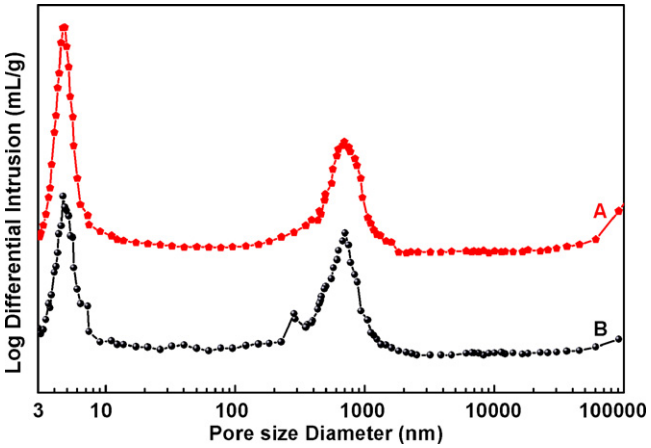


**Fig. 8.** MIP PSD of (A) CDH-0 and (B) CDH-4.

tion covered part of the active sites, while the pore structure of the catalysts was only slightly changed. Thus, it can be considered that the deactivated catalysts can be regenerated by burning-off the coke. The regeneration of the long-chain-paraffin dehydrogenation catalysts was not proposed by UOP Company [1], and little was reported on the industrial regeneration of this type of catalysts. Recently, in our research group, the studies on the regeneration of the long-chain-paraffin dehydrogenation catalysts have been carrying out [5,6]. The performance of the regenerated catalysts after the coke burning-off can be only recovered to 95% of that of the fresh catalysts. While the performance of the regenerated catalysts after the coke burning-off followed by the Pt modification can be recovered completely. Therefore, the regeneration technology of the long-chain-paraffin dehydrogenation catalysts has been suggested: programmed coke burning-off followed by the Pt modification. And the laboratory and pilot plant test is now undergoing.

## 4. Conclusions

The characterization of coke deposited on spent catalysts for long-chain-paraffin ($n$-$C_{16-19}$) dehydrogenation has been investigated in this study. It can be concluded that the dehydrogenation operation conditions (such as TOS and temperature) affect the coke deposition on the catalysts. With the prolongation of the dehydrogenation reaction, the amount of coke deposition on the catalysts and the graphitization degree of the coke are increased, and the velocity of carbon formation and the H/C mole ratio of coke are decreased. The coke is the deep-dehydrogenated carbonaceous compounds, which includes conjugated olefinic species and PAHs. The coke decreases the surface area and the total pore volume of the catalysts, and slightly narrows the pore size to smaller values.

## Acknowledgments

Yanli He, Zhaochi Feng, Xuming Wei and Fei Lv are acknowledged for the technical support and useful discussion during the catalyst characterizations.

## References

[1] M.M. Bhasin, J.H. McCain, B.V. Vora, T. Imai, P.R. Pujado, Dehydrogenation and oxydehydrogenation of paraffins to olefins, Appl. Catal. A: Gen. 221 (2001) 397–419.
[2] W. Wei, Y.H. Sun, B. Zhong, Catalytic dehydrogenation of a mixture of $C_{10}$–$C_{14}$ n-paraffins to linear $C_{10}$–$C_{14}$ monolefins in a supercritical phase, Chem. Commun. (1999) 2499–2500.
[3] S. He, C. Sun, H. Du, X. Dai, B. Wang, Effect of carbon addition on the Pt-Sn/gamma-$Al_2O_3$ catalyst for long chain paraffin dehydrogenation to olefin, Chem. Eng. J. 141 (2008) 284–289.
[4] S. He, C. Sun, Z. Bai, X. Dai, B. Wang, Dehydrogenation of long chain paraffins over supported Pt-Sn-K/$Al_2O_3$ catalysts: a study of the alumina support effect, Appl. Catal. A: Gen. 356 (2009) 88–98.
[5] S. He, Studies on the catalysts and the coke deposition behavior of the dehydrogenation of long chain paraffins ($C_{10}$–$C_{19}$), in: Chemical Engineering, Dalian Institute of Chemical Physics, Chinese Academy of Sciences, Dalian, 2009, pp. 1–198.
[6] J. Li, Studies on the regeneration of long-chain paraffin dehydrogenation catalyst, in: Chemical Engineering, Dalian Institute of Chemical Physics, Chinese Academy of Sciences, Dalian, 2006, pp. 1–85.
[7] D. Espinat, E. Freund, H. Dexpert, G. Martino, Localization and structure of carbonaceous deposits on reforming catalysts, J. Catal. 126 (1990) 496–518.
[8] J.M. Parera, R.J. Verderone, C.A. Querini, Coking on bifunctional catalysts, in: B. Delmon, G.F. Froment (Eds.), Catalyst Deactivation 1987, Elsevier Science Publ B.V., Amsterdam, 1987, pp. 135–146.
[9] N.A. Gaidai, S.L. Kiperman, Kinetic models of catalyst deactivation in paraffin dehydrogenation, Kinet. Catal. 42 (2001) 527–532.
[10] P. Gallezot, C. Leclercq, J. Barbier, P. Marecot, Location and structure of coke deposits on alumina-supported platinum catalysts by EELS associated with electron microscopy, J. Catal. 116 (1989) 164–170.
[11] N. Martin, M. Viniegra, R. Zarate, G. Espinosa, N. Batina, Coke characterization for an industrial Pt-Sn/-gamma-$Al_2O_3$ reforming catalyst, Catal. Today 107–108 (2005) 719–725.
[12] J. Barbier, Deactivation of reforming catalysts by coking – a review, Appl. Catal. 23 (1986) 225–243.
[13] J.C. Afonso, M. Schmal, R. Frety, The chemistry of coke deposits formed on a Pt-Sn catalyst during dehydrogenation of N-alkanes to mono-olefins, Fuel Process. Technol. 41 (1994) 13–25.
[14] M. Guisnet, P. Magnoux, Organic chemistry of coke formation, Appl. Catal. A: Gen. 212 (2001) 83–96.
[15] L.W. Lin, T. Zhang, J.L. Zang, Z.S. Xu, Dynamic process of carbon deposition on Pt and Pt-Sn catalysts for alkane dehydrogenation, Appl. Catal. 67 (1990) 11–23.
[16] J.M. Parera, N.S. Figoli, E.M. Traffano, Catalytic action of platinum on coke burning, J. Catal. 79 (1983) 481–484.
[17] S.A. Bocanegra, A.A. Castro, A. Guerrero-Ruiz, O.A. Scelza, S.R. de Miguel, Characteristics of the metallic phase of Pt/$Al_2O_3$ and Na-doped Pt/$Al_2O_3$ catalysts for light paraffins dehydrogenation, Chem. Eng. J. 118 (2006) 161–166.
[18] J. Margitfalvia, P. Szedlacseka, M. Hegedüsa, F. Nagya, Reaction kinetic approach to study activity, selectivity and deactivation of Pt/$Al_2O_3$ in n-hexane conversion, Appl. Catal. 15 (1985) 69–78.
[19] M. Bowker, T. Aslam, M. Roebuck, M. Moser, The effect of coke lay-down on n-heptane reforming on Pt and Pt-Sn catalysts, Appl. Catal. A: Gen. 257 (2004) 57–65.
[20] C.L. Pieck, C.R. Vera, C.A. Querini, J.A. Parera, Differences in coke burning-off from Pt-Sn/$Al_2O_3$ catalyst with oxygen or ozone, Appl. Catal. A: Gen. 278 (2005) 173–180.
[21] P. Praserthdam, N. Grisdanurak, W. Yuangsawatdikul, Coke formation over Pt-Sn-K/$Al_2O_3$ in $C_3$, $C_5$–$C_8$ alkane dehydrogenation, Chem. Eng. J. 77 (2000) 215–219.
[22] P. Marecot, A. Akhachane, C. Micheaud, J. Barbier, Deactivation by coking of supported palladium catalysts. Effect of time and temperature, Appl. Catal. A: Gen. 169 (1998) 189–196.
[23] N.S. Figoli, J.N. Beltramini, E.E. Marinelli, M.R. Sad, J.M. Parera, Operational conditions and coke formation on Pt-$Al_2O_3$ reforming catalyst, Appl. Catal. 5 (1983) 19–32.
[24] P. Praserthdam, T. Mongkhonsi, S. Kunatippapong, B. Jaikaew, N. Lim, Determination of coke deposition on metal active sites of propane dehydrogenation catalysts, in: C.H. Bartholomew, G.A. Fuentes (Eds.), Catalyst Deactivation 1997, Elsevier Science Publ B.V., Amsterdam, 1997, pp. 153–158.
[25] R.T. Baker, P.S. Harris, Chemistry and Physics of Carbon, Marcel Dekker, New York, 1978, pp. 83–165.
[26] H.P. Rebo, E.A. Blekkan, L. Bednarova, A. Holmen, Deactivation of Pt-Sn catalyst in propane dehydrogenation, in: B. Delmon, G.F. Froment (Eds.), Catalyst Deactivation 1999, Elsevier Science Publ B.V., Amsterdam, 1999, pp. 333–340.
[27] T. Zhang, J. Zang, L. Lin, Relation between surface structure and carbon deposition on Pt/$Al_2O_3$ and Pt-Sn/$Al_2O_3$ catalysts, in: C.H. Bartholomew, J.B. Butt (Eds.), Catalyst Deactivation 1991, Elsevier Science Publ B.V., Amsterdam, 1991, pp. 143–150.
[28] S.K. Sahoo, P.V.C. Rao, D. Rajeshwer, K.R. Krishnamurthy, I.D. Singh, Structural characterization of coke deposits on industrial spent paraffin dehydrogenation catalysts, Appl. Catal. A: Gen. 244 (2003) 311–321.
[29] Z.S. Xu, T. Zhang, Y.N. Fang, L.W. Lin, Carbon deposition and migration on Pt and Pt-Sn catalysts, in: C. Li, Q. Xin (Eds.), Spillover and Migration of Surface Species on Catalysts, Elsevier Science Publ B.V., Amsterdam, 1997, pp. 425–432.
[30] J. Barbier, Coking of reforming catalysts, in: B. Delmon, G.F. Froment (Eds.), Catalyst Deactivation 1987, Elsevier Science Publ B.V., Amsterdam, 1987, pp. 1–19.
[31] A.C. Ferrari, J. Robertson, Resonant Raman spectroscopy of disordered, amorphous, and diamondlike carbon, Phys. Rev. B 64 (2001) 075414.
[32] L. Lin, W. Lin, Y.X. Zhu, B.Y. Zhao, Y.C. Xie, G.Q. Jia, C. Li, Uniformly carbon-covered alumina and its surface characteristics, Langmuir 21 (2005) 5040–5046.
[33] J. Li, G. Xiong, Z. Feng, Z. Liu, Q. Xin, C. Li, Coke formation during the methanol conversion to olefins in zeolites studied by UV Raman spectroscopy, Microporous Mesoporous Mater. 39 (2000) 275–280.
[34] F. Negri, C. Castiglioni, M. Tommasini, G. Zerbi, A computational study of the Raman spectra of large polycyclic aromatic hydrocarbons: toward molecularly defined subunits of graphite, J. Phys. Chem. A 106 (2002) 3306–3317.
[35] Z. Xu, J. Zang, T. Zhang, Study of the carbonaceous deposition on Pt/$Al_2O_3$ catalysts by temperature programmed oxidation, Chin. J. Catal. 7 (1986) 230–236.
[36] T. Zhang, Study of the carbon depositiopn on highly disperd Pt/$Al_2O_3$, Pt-Sn/$Al_2O_3$ catalysts for the dehydrogenation of alkanes, in: Chemistry, Dalian Institute of Chemical Physics, Chinese Academy of Sciences, Dalian, 1989, pp. 1–163.
[37] C.L. Li, O. Novaro, E. Munoz, J.L. Boldu, X. Bokimi, J.A. Wang, T. Lopez, R. Gomez, Coke deactivation of Pd/H-mordenite catalysts used for $C_5$/$C_6$ hydroisomerization, Appl. Catal. A: Gen. 199 (2000) 211–220.
[38] K.S.W. Sing, D.H. Everett, R.A.W. Haul, L. Moscou, R.A. Pierotti, J. Rouquerol, T. Siemieniewska, Reporting physisorption data for gas/solid systems with special reference to the determination of surface area and porosity (Recommendations 1984), Pure Appl. Chem. 57 (1985) 603–619.
[39] S. Gomez, O. Giraldo, L.J. Garces, J. Villegas, S.L. Suib, New synthetic route for the incorporation of manganese species into the pores of MCM-48, Chem. Mater. 16 (2004) 2411–2417.
[40] M. Guisnet, "Coke" molecules trapped in the micropores of zeolites as active species in hydrocarbon transformations, J. Mol. Catal. A: Chem. 182–183 (2002) 367–382.